

The electron microscopy and crystallography of atomically constrained 1D crystals formed within single walled carbon nanotubes

Jeremy Sloan^{1,2}

¹Inorganic Chemistry Laboratory, University of Oxford, South Parks Road, Oxford, OX1 3QR UK ²Department of Materials, University of Oxford, South Parks Road, Oxford, OX1 3PH UK

Abstract:

The insertion behaviour of molecules and crystal growth of solid phase materials encapsulated within single walled carbon nanotubes (SWNTs) as elucidated by electron microscopy is reviewed. As SWNTs form within a strictly limited diameter range, their internal van der Waals surface controls the alignment of molecules and also the crystal growth behaviour of materials very precisely. Molecules either fit snugly into the SWNTs or may form aggregated clusters if they are significantly smaller than the internal cross-sectional volume defined by the internal van der Waals surface. Crystalline growth within SWNTs is atomically regulated and architectures of crystals that are integral atomic layers in thickness are possible. The structural properties of the resulting 1D crystals are dictated to some extent by the structural chemistry of the bulk material although deviations from bulk crystal growth behaviour are often observed and in a few instances crystals with completely new structures can form inside SWNTs. Nearly all crystals form with reduced surface coordination and exhibit lattice expansions or contractions as a result of reduction in coordination and/or van der Waals constriction within SWNTs.

Introduction¹:

We have studied the synthesis, characterisation and modification of individual molecules, one-dimensional crystals and other species formed within single walled carbon nanotubes (SWNTs) by conventional and restored high-resolution transmission electron microscopy (HRTEM). It has been possible to image the encapsulated species as either discrete molecules; one-dimensional arrays, helical chains and clusters of molecules; disordered or glassy filling; randomly orientated clusters or continuously aligned or helically distorted one-dimensional crystals. In the case of the latter, the crystals are constrained in cross-section by the van der Waals surface of the

¹ This paper is part of a lecture presented at the European Microscopy Congress 23.8.2005, Antwerp.

encapsulating SWNTs forming so-called 'Feynman Crystals' effectively integral numbers of atomic layers in terms of their thickness, specified by the diameter of the encapsulating tubule [1]. The ability of carbon nanotubes, in particular SWNTs, to 'fix' individual molecules or discrete crystals as small as 2-3 atomic layers in thickness for direct imaging is fostered by their extremely small internal diameters which exist within a very restricted range of ca. 0.4-5 nm with a median range of only 1-2 nm. When the van der Waals surface of the wall carbons is included then the internal diameters of the SWNT capillaries are further reduced by ~0.35 nm on average.

These nanocomposite materials represent a new generation of materials that can be synthesised on a bulk scale and that can potentially form the basis of diodes [2-4], single electron transistors [5,6], memory elements [7] and logic circuits [8] and recently, substantial progress has been made with respect to the comprehensive characterisation of these remarkable nanocomposites. Of particular importance must be considered to be: (i) the component crystal structure of the encapsulating nanotubes which may be conveniently reduced to the (n,m) chiral indices defining the sp^2 carbon cylinder according to the equation $\mathbf{C}_h = n\mathbf{a}_1 + m\mathbf{a}_2$, where \mathbf{C}_h is the roll-up vector and \mathbf{a}_1 and \mathbf{a}_2 are the basal vectors of the parent 2D carbon lattice, and (ii) the conformation, packing behaviour or crystal structure of the encapsulated molecules and/or 1D crystal structures. This paper will highlight some of the more significant developments that have been made with regard to the complete characterisation of SWNT nanocomposites.

SWNT Encapsulation Methodologies

The first crystalline insertions observed within SWNTs were clusters of Ru metal formed by immersing a sample of acid-treated SWNTs in a saturated solution of RuCl_3 [9]. Subsequently, SWNTs were filled by capillary wetting with molten mixtures of silver halides or mixtures of alkali and actinide halides [10]. The ability of a molten material to wet and fill SWNTs depends on the wetting criterion determined by Ebbesen for the filling of nanotubes with liquid phase media [11]. In general, the filling procedure entails heating as-made nanotubes with the molten salt or oxide to a temperature 100K above the respective melting point. Improvements in filling yield can be achieved by thermally cycling the filling material between the filling temperature and 100K below this temperature [12]. Mixtures of predominantly amorphous ternary phase materials may be introduced into SWNTs by exploiting the melting properties of the relevant phase diagram [10]. SWNTs can now be filled with a wide range of materials including metals and metal salts [1,9,10], oxides [13,14], helical iodine chains [15].

Further modifications are possible on such materials once they are incorporated within SWNTs. For example, with SWNTs filled with silver halides, the halide undergoes spontaneous photolytic decomposition resulting in the formation of aligned 1D fcc silver nanowires [10]. Similarly, it has been possible to reduce incorporated RuCl_3 to the base metal (see above) and formation of reduced lanthanide nanowires has also been

reported [16].

In addition to the incorporation of crystalline or non-crystalline materials into SWNTs, it has also been possible to insert and directly image molecular structures within their capillaries. The first such imaged species were C_{60} molecules formed within nanotubes produced by laser ablation resulting in SWNT composite structures called 'peapods' [17] (Fig 1(a) and (b)). Quantitative filling of SWNTs with fullerenes [18,19] or endofullerenes [20] has since been effected by gas phase diffusion heat-treated SWNT samples. More recently, non-fullerene molecular species have been inserted into SWNTs. These include metallocenes, molecular halides and *ortho*-carborane molecules (Fig. 1(c) to (g)) [21,22].

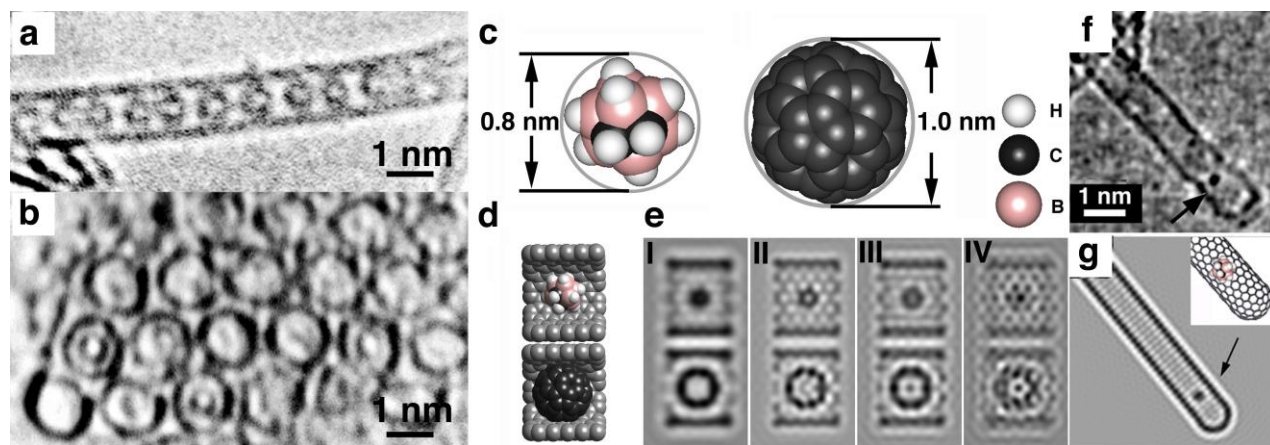


Fig. 1 (a) HTEM image, obtained at 100 kV showing the first example of a SWNT filled with C_{60} molecules. (b) Second image from the same specimens as in (a) showing a cross-sectional view of an ordered bundle of SWNTs some of which are filled with fullerenes. (c) structure models indicating the outside diameters of *o*-carborane (left) and C_{60} (right). (d) and (e) packing models and corresponding focal series images showing the different imaging properties of *o*-carborane (top) and C_{60} inside fragments of (10,10) SWNTs. (f) and (g) HRTEM image and corresponding image simulation (with model inset) showing a single *o*-carborane molecule formed within the tip of a SWNT.

Characterisation of SWNT encapsulates by electron diffraction

As described in the previous section, the self-organisation of fullerene molecules along SWNT capillaries leads to the formation of one-dimensional crystals. Electron diffraction and direct imaging techniques can be utilised to extract information from individual filled SWNTs. Recent work has shown that semi-quantitative analysis of selected area electron diffraction (SADP) patterns obtained from unfilled DWNTs and which in principle permit retrieval of the chiral indices of the component tubules for nanotubes of diameters up to 40 Å (i.e. 4 nm) in diameter [23]. This approach is essentially an extension of similar diffraction experiments originally implemented to establish the chiral nature of multi-

walled nanotubes [24] and consists of extracting diffraction intensities from patterns obtained using a high-coherence field emission gun (i.e. FEG) electron source. Simulation of the diffracted intensity for all possible component (n,m) SWNTs and extensive comparison of these intensities with kinematic theory suggested that the component chiral indices of the two constituent nanotubes could be retrieved with reasonable precision [23]. Similar results were reported for localized regions of SWNTs using nanoarea electron diffraction [25]. In an even more remarkable experiment, Zuo et al. showed that it is possible to extract the phase information from DWNT SADPs with the result that the 2D crystal structure of the parent nanotube can be reconstructed in an approach analogous to the solution of the phase problem in X-ray crystallography [26]. With respect to the interpretation of SWNT-incorporated species, direct electron diffraction measurements have predominantly been confined to determining the lattice spacings within 1D crystals of incorporated fullerene molecules within peapod encapsulates. Selected area electron diffraction (SADP) pattern measurements from bundles of SWNTs filled with different size and shape fullerenes have so far shown that the inter-molecule separations are in fact 3-4% smaller than those measured for the corresponding bulk fullerene crystals [27] in which the molecules are separated by slightly less than the van der Waals graphene separation (ca. 0.34 nm).

Imaging of encapsulated species by conventional and restored HRTEM

Direct lattice imaging by conventional HRTEM can be used to image both molecular species and aligned 1D crystals formed within SWNTs. Indeed, the technique has proved invaluable since both the microstructure and helical nature of multilayer nanotubes was correctly demonstrated by a combination of HRTEM and electron diffraction in 1993 [28]. More recently, considerable progress has been made with regard to the direct and super-resolved and spectroscopic imaging of SWNT-incorporated molecules and 1D crystals. With respect to the imaging of species formed within SWNTs by HRTEM, five considerations are paramount with respect to obtaining the maximum level of information: (i) the spatial resolution of the imaging technique being used; (ii) the imaging properties of the encapsulated specimen; (iii) the structural chemistry of the incorporated specimen and the encapsulating nanotube (iv) the relative stability of the encapsulated specimen with respect to the imaging technique and conditions being used, and (v) the degree of 3D information that may be obtained from the respective technique. As shown below, it is possible to extrapolate (v) from certain kinds of information available in 2D projections of directly imaged specimens but there still needs to be further advances in instrument design before true 3D information will be available at the atomic level. The spatial resolution of a HRTEM is principally governed by the quality of the main imaging objective lens and may be expressed in terms of the spherical aberration coefficient (C_s). The consequence for conventional HRTEM is that the point resolution is reduced to between 0.16 and 0.3 nm for most commercial instruments. It is possible with

such resolution to 'see' individual strongly scattering atoms and ordered columns or clusters of more weakly scattering atoms imaged in projection. In Fig. 2(a), for example, we see a conventional HRTEM images obtained at close to optimum Scherzer defocus conditions of a 2×2 KI crystal formed within an SWNT of ca. 1.4 nm in diameter (28). In this image, the I-K or K-I columns are clearly resolved (*cf.* structure model in Fig. 2(b)) whereas the graphene walls appear as continuous and featureless parallel black lines. Similarly, in the images and simulations of fullerenes and carborane molecules shown above (i.e. Fig. 1), the nanotubes image as parallel black lines and the encapsulated molecules either image as black circles, in the case of the fullerenes (Figs. 1(a)-(c)) or as indistinct blurred spots, as in the case of the carboranes (i.e. Figs. 1(c)-(e)). In these cases, the contrast is due to columns of superposed carbon or boron and carbon atoms. Under such imaging conditions information from columns of light elements is unavailable. In Fig 2(a) only the strongly scattering I columns ($Z = 53$) contribute significantly to the image contrast while the K atoms ($Z = 19$) make only a negligible contribution.

Considerable enhancement of the detail available from conventional HRTEM images may be made, providing that the sample is stable enough by restoring the exit plane-wave of the electron beam propagating from the specimen from either a tilt or focal series of HRTEM images [29-31]. In doing so, several key aberrations may be removed with the result that information out to or beyond the information limit rather than the point resolution (e.g. 0.1 nm as opposed to 0.16 nm for a JEOL 300 kV FEGTEM).

In Fig. 2(c), we see an example of a restored image of 3×3 KI formed within a ca. 1.6 nm diameter SWNT and in Fig. 2(d) the corresponding derived structure model [32]. As the encapsulated crystal is visible in a [110] projection relative to bulk KI, all the atom column are visible as pure atom columns. In the conventional image (not shown), the heavy I atoms are visible whereas the K atoms are invisible. In the case of the reverse contrast restored image (Fig. 1(c)), we see that the I columns are now much more prominent but are now interspersed with the weaker K columns. A further key point is that the intensities of the bright spots corresponding to pure I and K columns are modulated according to atom column thickness. Thus, along the SWNT we can easily identify two alternating layers corresponding to I-2K-3I-2K-I and K-2I-3K-2I-K, consistent with the 3×3 KI crystal. It is noteworthy that both 1D crystals display considerable lattice distortions compared to their bulk structures. In the 2×2 case, a lattice expansion of ca. 17% occurs across the SWNT capillary whereas in the 3×3 case a differential expansion is observed with the I columns being more compressed than the K columns (see Fig. 2(d)).

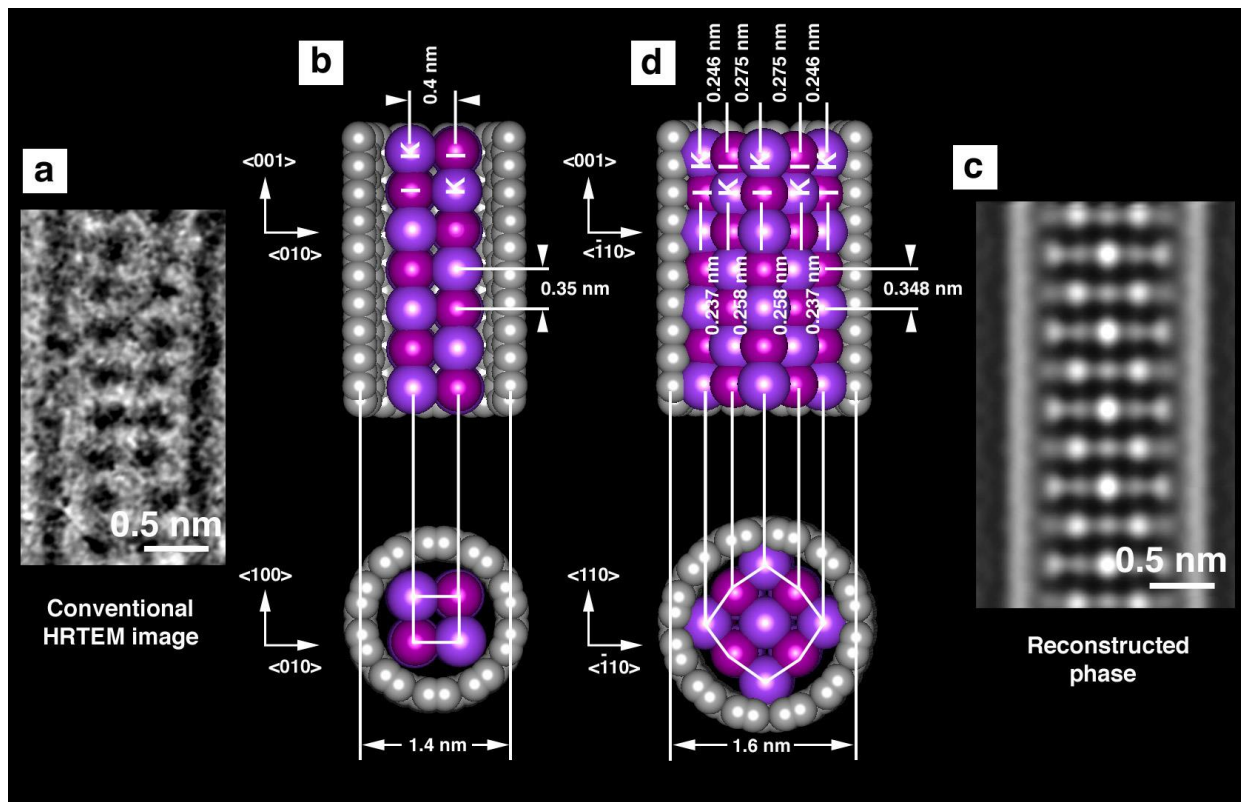


Fig. 2 (a) Conventional HRTEM image of a 2×2 KI crystal formed within a ca. 1.4 nm diameter SWNT. (b) Structure model derived from (a). (c) Super-resolved HRTEM image of a 3×3 KI ca. 1.6 nm diameter SWNT. (d) Structure model derived from (c).

Another advantage of the focal series technique is that, by restoring sub-regions of a composite image, the relative height of each sub-region relative to each contiguous sub-region can be computed giving a measure of the relative tilt of the SWNT HRTEM (14). Under favourable conditions, this information can be combined with imaging information obtained from the SWNT walls that provides information about the conformation of the encapsulating SWNT. In Fig. 3(a), we can see a restored image of A 1D crystal of Sb_2O_3 formed within a ca. 1.45 nm diameter SWNT. By examining the image and the absolute focus level along the length of the SWNT (see right hand plot, Fig 3(a)), we can easily establish that this is a tilted SWNT and that the angle of tilt with respect to the plane of the image is ca. 15° . In addition to this information, we can also see that at the bottom of the image that the encapsulated 1D crystal is resolved as a 2D array of atom columns and that along indicated direction **1**, that wall carbons columns, with spacing of 0.224 nm, are clearly visible. No such contrast is evident on the left hand wall, indicated by **2**. The spatial frequencies along the nanotube walls were extracted accurately from 1D power spectra (Fig. 3(b)) and these were exhaustively compared against spatial frequencies

computed for all SWNTs having diameters in a similar range to the experimental case. A candidate tube with a conformation of (21,-8) (being the mirror image of (13,8)) was chosen in order to simulate the experimental case (Fig. 3(c)). Analysis of both the carbon wall contrast and the nanotube tilt gives us unambiguously the *handedness* of a chiral SWNT. The obtained crystal structure corresponded to a 1D fragment extracted from the valentinite form of Sb_2O_3 as opposed to the senarmorite form (Fig. 3(d)) which was used to simulate the structure (Fig. 3(e)). In this instance, we have only been able to resolve the strongly scattering Sb^{3+} columns while the O^{2-} columns were lost in the image noise. The column thicknesses of the former (*cf.* Fig. 2(c)) were measured to be 3-3-2-3-3.

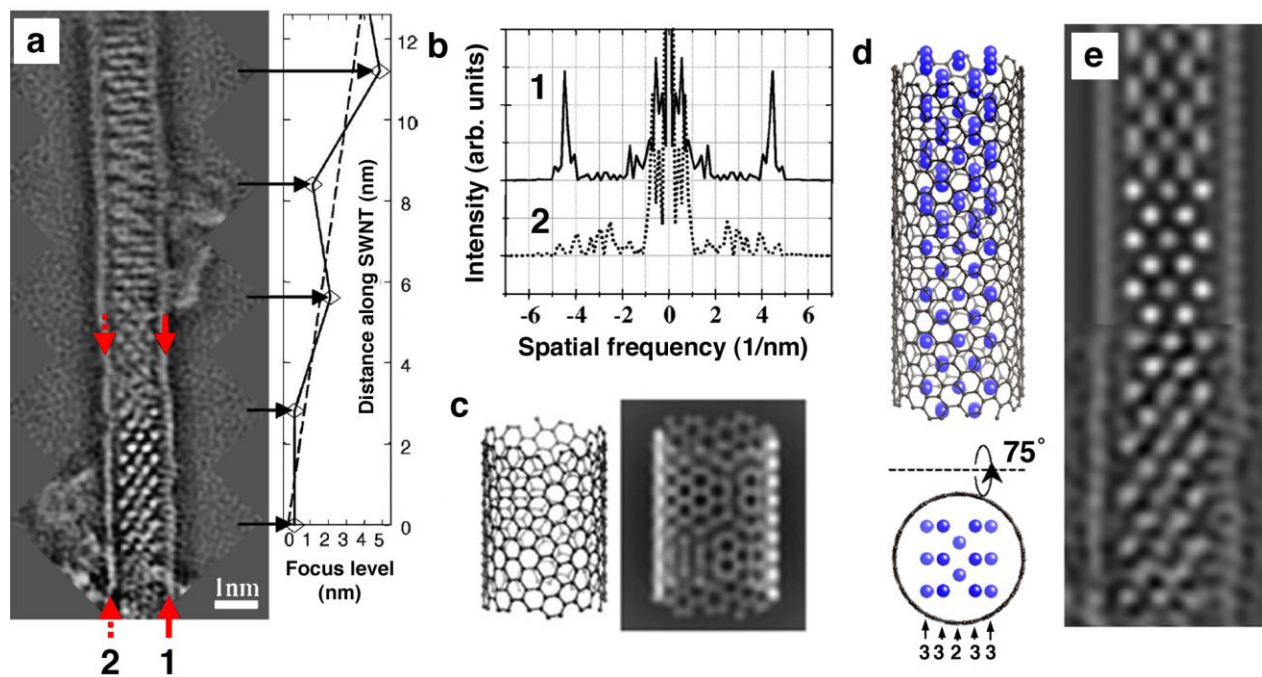


Fig. 3 (a) Restored HRTEM phase image recorded from a $\text{Sb}_2\text{O}_3/\text{SWNT}$ nanocomposite. At right is a plot of focus level versus distance along the SWNT. (b) 1D power spectra obtained from the two opposing walls (i.e. **1** and **2** in (a)) of the SWNT. (c) Derived conformation and simulation of the encapsulating SWNT in (a). (d) Structure model of encapsulate (Sb atoms indicated in blue). (e) Comparison of multislice simulation produced from (d) (top) and experimental image (bottom).

In both previous examples, we can extract some cues concerning the three dimensional nature of the SWNT encapsulates from the presumed geometry of the nanotube, the phase shifts observed for individual atom columns and also from the measured tilt angle of the nanotube. This is relatively easy for comparatively symmetrical 1D crystals (e.g. KI) but quite difficult for more asymmetric cases. In the special case of a twisted 1D crystal,

however, we can extract the entire 1D crystal structure providing that the same microstructure is maintained along the imaged length of the nanocomposite [37]. In Fig. 4(a), we see the reconstructed phase of a distorting SWNT continuously filled with Co_2I_4 .

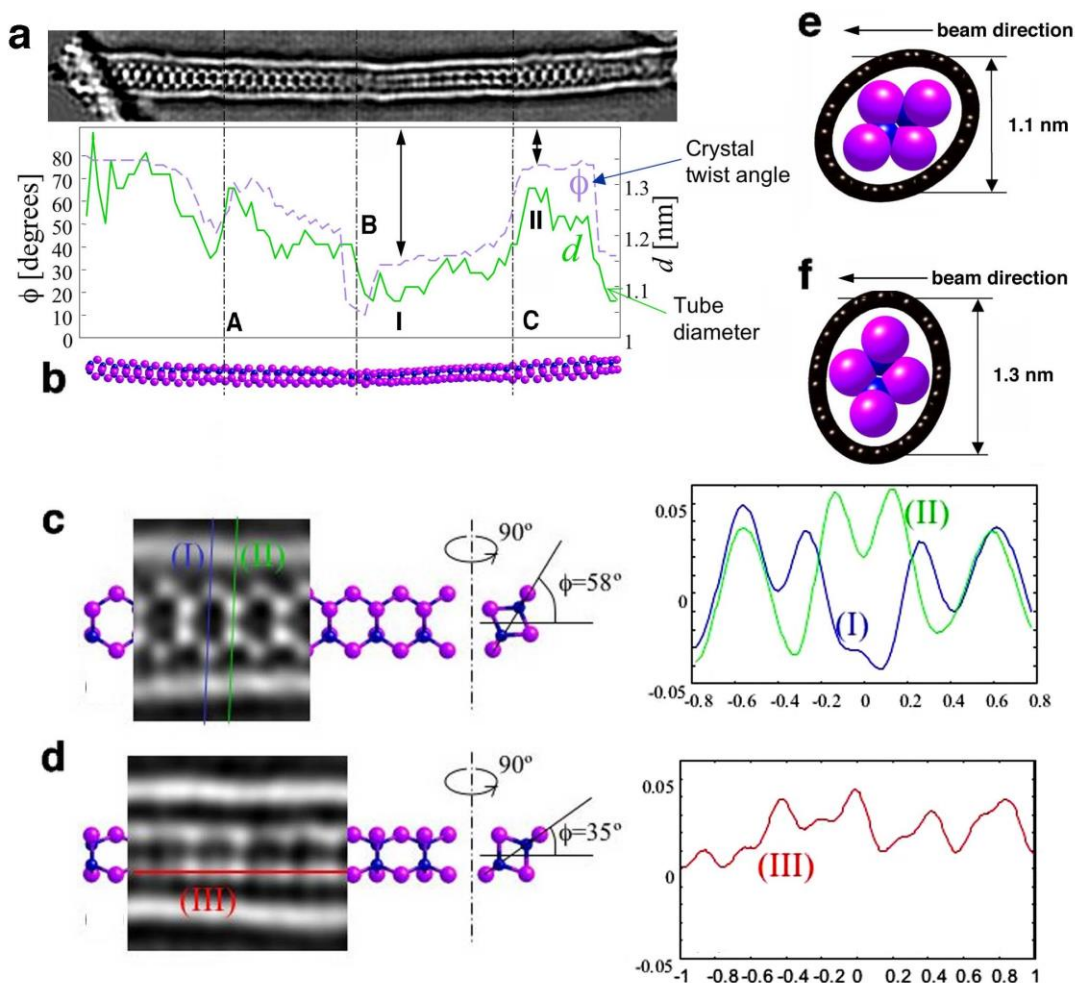


Fig. 4 (a) Restored HRTEM phase image produced from a composite between a 1D Co_2I_4 crystal and a distorting SWNT. The plot shows the variation of SWNT diameter (**d**) together with the angle of rotation (ϕ) of the Co_2I_4 motif within the encapsulated 1D crystal. (b) Derived structure model. (c) and (d) details from left and right middle sections of (a) showing the microstructure of the 1D crystal in two the different projections effected by the crystal rotation. Line profiles (at right or (c) and (d)) through I, II and III were used to confirm the whole crystal structure of the twisting fragment. (e) and (f) end on views of Co_2I_4 units in two different orientations. The diamond shape of the Co_2I_4 motif causes an oval distorting in the encapsulating nanotube.

Detailed analysis of the structure of this fragment (model shown in Fig. 4(b)) shows that it differs considerably from the bulk form of the iodide which can be described as stacked 2D layers of edge-sharing CoI_6 octahedra. Figs. 4(c) and (d) shows two details obtained from the reconstructed phase shows a chain of pairs of atom columns, separated by 0.54nm and 0.26 nm perpendicularly to the SWNT axis, respectively. Inspection of the whole fragment along the indicated regions **A**, **B** and **C** in Fig. 4(a) suggest that this same microstructure is maintained along the length of the nanocomposite. Single pixel width line profiles at **I**, **II** and **III** were used to produce an accurate 3D picture of the whole structure which is consistent with a Co_2I_4 repeating unit with the central columns along **II** corresponding to I-Co and Co-I columns with the peripheral atom columns measured along **I** corresponding to single I columns, only. It can be seen that this fragment rotates in a fairly smooth fashion along the SWNT capillary (although there is an abrupt rotation at **B**, Fig. 4(a)), given by the indicated angle ϕ in Figs. 4(a), (c) and (d). A further remarkable feature of this composite is that the asymmetric CoI_2 encapsulate causes a corresponding distortion in the encapsulating nanotube and, further, that this distortion rotates as the Co_2I_4 rotates along the length of the SWNT (Fig. 4(e) and (f)). The correlation between ϕ and d is plotted in Fig. 4(a).

Acknowledgements

The author is grateful to the contributions of numerous collaborators from Oxford and elsewhere. In particular I am grateful to Prof. A. I. Kirkland, Dr. J. L. Hutchison, Dr. R. R. Meyer, Prof. M. L. H. Green, Dr. E. Philp, D.A. Morgan, Dr. R. Carter, Dr. P.M.F.J. Costa, Dr. G. Brown, Dr. S.R. Bailey, Dr. S. Friedrichs, Dr. E. Flahaut (now at CNRS, Toulouse), Dr. R.E. Dunin-Borowski and Dr. O. Saxton from Cambridge University. I am grateful for financial support to the EPSRC, The Leverhulme Foundation and The Royal Society. I would also like to express my deep appreciation to FEI for sponsoring the FEI European Microscopy Award and Plenary Lecture from which this paper is derived.

References

- [1] J. Sloan et al., *Integral atomic layer architectures of 1D crystals inserted into single walled carbon nanotubes*, Chem. Commun. (2002) pp. 1319-1332.
- [2] Y. Zhen et al., *Carbon nanotube intramolecular junctions*, Nature (1999), **402**, pp. 273-274.
- [3] R.D. Antonov, and A.T. Johnson, *Subband population in a single-wall carbon nanotube diode*, Phys. Rev. Lett. **83** (1999) pp. 3274-3276.
- [4] C. Zhou et al. *Modulated chemical doping of individual carbon nanotubes*, Science **290** (2000) pp. 1552-1555.

- [5]S. J. Tans, A. R. M. Verschueren, and C. Dekker, *Room-temperature transistor based on a single carbon nanotube*, Nature, **333** (1998) pp. 49-52.
- [6]H.W. Ch. Postma et al., Carbon nanotube single-electron transistors at room temperature, Science **293** (2001) pp. 76-79.
- [7]T. Rueckes, *Carbon nanotube-based nonvolatile random access memory for molecular computing.*, Science **289** (2000) pp. 94-97.
- [8] A. Bachtold, *Logic circuits with carbon nanotube transistors*, Science **294** (2001) pp. 1317-1320.
- [9] J. Sloan et al., *Opening and filling single walled carbon nanotubes (SWTs)*, Chem. Commun., (1998) pp. 347-347.
- [10]J. Sloan et al., *Capillarity and silver nanowire formation observed in single walled carbon nanotubes*, Chem. Commun., (1999) pp. 699-700.
- [11] T.W. Ebbesen, *Wetting, filling and decorating carbon nanotubes*, J. Phys. Chem. Solids, **57** (1996) pp. 951-955.
- [12]G. Brown et al., *High yield incorporation and washing properties of halides incorporated single walled carbon nanotubes*, Appl. Phys. A, **76** (2003) pp. 1-6.
- [13]J. Mittal et al., *Room temperature filling of single-wall carbon nanotubes with chromium oxide in open air*, Chem. Phys. Lett., **339** (2001) pp. 311-318.
- [14]S. Friedrichs et al., *Simultaneous determination of inclusion crystallography and nanotube conformation for a Sb_2O_3 /single-walled nanotube composite*, Phys. Rev. B, **64** (2001) pp. 045406/1-8.
- [15]X. Fan et al. *Atomic Arrangement of Iodine Atoms inside Single-Walled Carbon Nanotubes*, Phys. Rev. Lett., **84** (2000) pp. 4621-4624.
- [16]B.C. Satishkumar, *Filling single-wall carbon nanotubes with d- and f-metal chloride and metal nanowires*, J. Nanosci. Nanotech. **3** (2003) pp. 159-163.
- [17]B.W. Smith, M. Monthieux, and D.E. Luzzi, *Encapsulated C_{60} in carbon nanotubes*, Nature, **396** (1998) pp. 323-324.

- [18]B. W. Smith et al., *High-yield synthesis and one-dimensional structure of C₆₀ encapsulated in single-wall carbon nanotubes*, J. Appl. Phys. **91** (2002) pp. 9333-9340.
- [19]H. Kuzmany et al. *Analysis of the concentration of C₆₀ fullerenes in single wall carbon nanotubes*, Appl., Phys. A, **76** (2003) pp. 449-456.
- [20]K. Hirahara et al., *One-dimensional metallofullerene crystal generated inside single-walled carbon nanotubes*, Phys. Rev. Lett., **85** (2000) pp. 5384-5387.
- [21] F. Stercel et al., *Single wall carbon nanotubes filled with metallocenes: a first example of non-fullerene peapods*, MRS Proceedings, **706** (2002), pp. 245-250.
- [22]D.A. Morgan, J. Sloan and M.L.H. Green, *Direct imaging of o-carborane molecules within single walled carbon nanotubes*, Chem. Commun., (2002) pp. 2442-2443.
- [23]M. Kociak et al., *How accurate can the determination of chiral indices of carbon nanotubes be? An experimental investigation of chiral indices determination on DWNT by electron diffraction*, Eur. Phys. J. B., **32** (2003) pp. 457.
- [24]S. Iijima, *Helical microtubules of graphene carbon*, Nature, **345** (1991) pp. 56-58.
- [25]M. Gao et al., *Structure determination of individual single-wall carbon nanotubes by nanoarea electron diffraction*, Appl. Phys. Lett. **82** (2003) 2703-2705.
- [26]J. M. Zuo et al., *Atomic Resolution Imaging of a Carbon Nanotube from Diffraction Intensities*, Science, **300** (2003) pp.1419-1421.
- [27]K. Hirahara, *Electron diffraction study of one-dimensional crystals of fullerenes*, Phys. Rev. B **64** (2001) pp. 115420/1-5.
- [28]J. Sloan et al., *Two layer 4:4 co-ordinated KI crystals grown within single walled carbon nanotubes*, Chem. Phys. Lett., **329** (2000) pp. 61-65.
- [29]A.I. Kirkland, W.O. Saxton, and G. Chand, *Multiple beam tilt microscopy for super resolved imaging*, J. Electron Microsc. **46** (1997) pp. 11-22.
- [30]W. Coene et al., *Phase retrieval through focus variation for ultraresolution in field-emission transmission electron microscopy*, Phys. Rev. Lett., **69** (1992) pp. 3743-3746.

- [31] R.R. Meyer, A.I. Kirkland, and W.O. Saxton, *A new method for the determination of the wave aberration function for high resolution TEM 1. Measurement of the symmetric aberrations.*, *Ultramicroscopy*, **92** (2002) pp. 89-109.
- [32] R.R. Meyer et al., *Discrete atom imaging of one-dimensional crystals formed within single walled carbon nanotubes*, *Science*, **289** (2000) pp. 1324-1326.
- [33] E. Philp et al., *An encapsulated helical 1D cobalt iodide crystal*, *Nature Mater.*, **2** (2003) pp. 788-791.